

Static spheres and Aschenbach effect for black holes in massive gravity

Pavan Kumar Yerra¹, Sudipta Mukherji² and Chandrasekhar Bhamidipati³

¹ Institute of Fundamental Physics and Quantum Technology,
Ningbo University, Ningbo, Zhejiang 315211, China

¹ School of Physical Science and Technology,
Ningbo University, Ningbo, Zhejiang 315211, China

^{1,2} Institute of Physics, Sachivalaya Marg, Bhubaneswar, Odisha, 751005, India

^{1,2} Homi Bhabha National Institute, Training School Complex,
Anushakti Nagar, Mumbai, 400085, India

³ Department of Physics, School of Basic Sciences,
Indian Institute of Technology Bhubaneswar, Bhubaneswar, Odisha, 752050, India

Abstract

In this paper, we study the trajectories of massive and massless particles in four dimensional static and spherically symmetric black holes in dRGT massive gravity theory via phase-plane analysis and point out several novel features. In particular, we show the existence of a static sphere, a finite radial distance outside the black holes in these theories, where a massive particle can be at rest, as seen by an asymptotic zero angular momentum observer. Topological arguments show that the stable and unstable static spheres, which come in pairs, have opposite charges. In the presence of angular momentum, we first study the behaviour of massless particles and find the presence of stable and unstable photon spheres in both neutral and charged black holes. Subsequently, we study the motion of massive test particles around these black holes, and find one pair of stable and unstable time-like circular orbits (TCOs), such that the stable and unstable TCO's are disconnected in certain regions. Computing the angular velocity Ω_{CO} of the TCOs, measured by a static observer at rest, shows the unusual nature of its monotonic increase with the radius of TCO, near the location of stable photon sphere. This confirms the existence of Aschenbach effect for spherically symmetric black holes in massive gravity, which was only found to exist in rapidly spinning black holes, with the only other exception being the rare example of gravity coupled to quasi-topological electromagnetism.

¹pk11@iitbbs.ac.in

²mukherji@iopb.res.in

³chandrasekhar@iitbbs.ac.in

1 Introduction

Investigation of orbits of particles is ubiquitous for uncovering novel observable gravitational phenomena and testing various features of compact objects in Einstein gravity as well as modified theories of gravity. Applications range from situations involving strong and weak gravitational effects around black holes, such as ring down in a binary system of black holes[1], shadows[2, 3], and to other interesting phenomena in four and higher dimensions, with potential observational signatures [4–11]. Stable circular orbits of massive particles around black holes can be used to study accretion discs, whereas unstable ones provide information about shadows. Certain physical quantities, such as Energy, angular momentum and angular velocity are generally examined to extract information about the orbital dynamics [12–27].

Lately, novel methods have been proposed for investigation of orbits of particles around static spherically symmetric, as well as rotating compact objects, accoutred with topological and geometrical techniques[19–27]. In other developments, with a view to unveiling unique signatures which could distinguish rotating objects such as Kerr black holes from other non-Kerr space-times (such as boson stars, wormholes etc.), the phenomena of static spheres has also been studied[23]. The idea is as follows. In a rotating space-time, particles can have orbits which are non-rotating, co-rotating or counter-rotating, depending on the sign and magnitude of their angular momentum. The later type of orbits are interesting, as they have negative angular momentum and might appear static, to an asymptotically static observer. Of course, the angular momentum of the particle has to be highly fine tuned, in addition to its location being the minimum of the potential. In static and spherically symmetric space-times, obtaining such static spheres is not straightforward, as massive test particles with zero angular momentum generally cannot be at rest around black holes under general conditions. For instance, the angular velocity of the object has to vanish at a finite radius, which does not occur in Einstein gravity coupled to standard matter, even for low black hole spins. However, motivated by recent studies on orbits around various black hole space-times[19–27], it was shown that such static spheres do exist in a rare example of gravity coupled to quasi-topological electromagnetism [28, 29], which can mimic Dyson sphere [30] (originally constructed around stellar structures[31, 32]). Considering that finding such static spheres in spherically symmetric gravitational systems could put to test various modified theories of gravity, it is imperative to look for further examples where such phenomena could occur.

Another related development which could be worthwhile to explore, especially, for testing modified theories of gravity, concerns an intriguing effect found by Aschenback[33], coming from the study of radial gradient of orbital velocity around rotating black hole space-times. Let us elaborate. Generally, in Newtonian mechanics, or even while studying orbits of massive particles around spherically symmetric and/or rotating black holes, the angular velocity increases monotonically with decreasing radius. This behaviour also continues to hold for small values of rotation a and large orbit radius r . What was found in[33] is that, for rapidly spinning black holes with $a > 0.9953$ (but still below the Thorne limit[34] $a = 0.998$), the radial gradient of orbital velocity can decrease with decreasing r in a narrow window of orbital radius, before resuming its normal increasing behaviour. This effect is very specific to zero angular momentum observers (ZAMOs) or so called Bardeen observers, and the results appear to be commensurate

with the high frequency quasi-periodic oscillations originating in the accretion disk of compact objects, such as from X-ray binaries. Considering the possibility of experimental observations, the Aschenbach effect has received increased attention with investigations extended to more general Kerr black holes[35–37], as well as when the particles are charged[38], and/or rapidly spinning [39, 40].

Now, since the Aschenbach effect occurs for test particles in orbits around rapidly spinning black holes[33, 35], as observed by ZAMOs, it was not expected to be present when the black hole is non-rotating (or slowly rotating). At least, this is what can be deduced for spherically symmetric black holes in Einstein gravity. However, recently, in the aforementioned model of Einstein gravity coupled to nonlinear electrodynamics, the Aschenbach effect was found to be present [29], aided by the occurrence of static spheres in a certain narrow range of charge to mass ratio of the black hole. As emphasised earlier, due to the possibility of potential experimentally observational signatures, the Aschenbach effect should be explored further, in more general settings, which could give rise to clues to the possible nature of the compact object. In this paper, we find a novel example where the Aschenbach effect can be present in a theory of massive gravity, which contains static and spherically symmetric black holes, with a rich structure of stable/unstable circular orbits of test particles. Our study is also expected to be helpful while exploring various lower bounds on physical quantities related to orbits of black holes[41], particularly, in massive gravity.

Following are some broad motivations for considering a massive theory of gravity. Einstein’s gravity has had high success with experimental observation of several of its predictions, buoyed further with the most recent evidences coming from the LIGO collaboration [42, 43] pertaining to gravitational wave signals. Notwithstanding these triumphs, there continue to be other phenomena of paramount importance, foremost being the accelerated expansion of the universe, and the longstanding cosmological constant problem, among others, necessitating exploration of modified theories of gravity. One of the possibilities explored concerns massive graviton theories, looked into with motivation from hierarchy problems and strong connections with quantum theory of gravity [44, 45], which is within the ambit of recent observations [46], where novel limits on the graviton mass are obtained. We should mention that, massive theories of gravity have a good history, with the first models being constructed as early as 1939 by Firez and Paullo [47]. These models of course have now undergone considerable modifications, most notably the the advent of new massive gravites[48–51] which are being investigated actively[52–58]. Black hole solutions in these theories have interesting thermodynamic phases [59–62] with wide ranging cosmology/astrophysics applications, which should be helpful in identifying deviations from Einstein’s theory [63–69]. Of interest to this work is an interesting class of massive theory of gravity proposed in [70], which has a well formulated holographic dual description. The model in [70] has a singular metric, with other useful features of stability and absence of ghosts[71], together with the presence of black holes[72–76]. There are considerable advantages in constructing such massive theories of gravity, which have the necessary ingredients for addressing some of the aforementioned issues as elaborated in [77–89]: to mention one, it may be possible to understand the current observations emanating from dark matter [90] and also correlating with the accelerating expansion of our universe where the requirement of dark energy component could

be relaxed [91, 92]. Let us also mention in passing, the continued efforts in embedding massive theories of gravity in the string theory framework [93]. Some recent developments in general theories of gravity are also on the thermodynamic front, where the cosmological constant is taken to a variable, giving rise to the concept of pressure and black hole chemistry program (see[94] and references therein), which has been explored extensively in massive gravity theories [75, 76, 95–102]. The issue of black hole microstructures in these theories have also been explored from the point of view of thermodynamic geometry with interesting results [103–109].

Rest of the paper is organised as follows. In section-(2), we present a brief overview of the static and spherically symmetric black holes in massive gravity in four dimensions. These black holes, often endowed with multiple horizons, have rich geometric structures. Consequently, motions of massive and massless particles around these black holes possess diverse trajectories, including that of the static spheres. To explore the nature of these trajectories, in section-(3), we develop a phase-plane analysis of the system. We find the fixed points and complete phase portraits, dictated by those fixed points. Owing to the fact that the black holes in massive gravity have several free parameters, our study in this section is not exhaustive. We fix some of these parameters and vary the rest in a way that captures qualitatively different geodesics. Subsequent section is devoted to examining one class of these geodesics associated with the massive particles, namely the static spheres. In section-(4.1), we present the conditions for the existence of circular orbits for massive test particles when the orbital angular momentum vanishes, and then proceed to count the number of such static spheres, based on topological arguments. Exploiting the presence of static spheres and stable photon spheres in the massive gravity, in section-(4.3), we study the Aschenback effect, where the angular velocity of a time-like circular orbit is found to be increasing with its radius coordinate under certain conditions. Finally, we conclude in section-(5).

2 Static & spherically symmetric black holes in massive gravity

We consider the dRGT massive gravity theory, where the action for a four dimensional Einstein-Maxwell gravity coupled to nonlinear interaction terms giving the graviton a mass m_g , can be written as ¹ [110–112]:

$$I = \frac{1}{16\pi} \int d^4x \sqrt{-g} \left(\mathcal{R} - \mathcal{F} + m_g^2 \mathcal{U}(g, \Phi^a) \right). \quad (2.1)$$

Here, \mathcal{R} is the Ricci scalar, and the Maxwell invariant $\mathcal{F} = F_{\mu\nu} F^{\mu\nu}$ with $F_{\mu\nu} = \partial_\mu A_\nu - \partial_\nu A_\mu$ is given in terms of the gauge potential A_μ . \mathcal{U} is the effective potential for graviton, and it has the following expression in four dimensional spacetime:

$$\mathcal{U}(g, \Phi^a) = \mathcal{U}_2 + \alpha_3 \mathcal{U}_3 + \alpha_4 \mathcal{U}_4,$$

where, α_3 and α_4 are dimensionless parameters which will be replaced by two new parameters, α and β , such that $\alpha_3 = \frac{\alpha-1}{3}$ and $\alpha_4 = \frac{\beta}{4} + \frac{1-\alpha}{12}$. The \mathcal{U}_i 's can be expressed as

$$\begin{aligned} \mathcal{U}_2 &\equiv [\mathcal{K}]^2 - [\mathcal{K}^2], \\ \mathcal{U}_3 &\equiv [\mathcal{K}]^3 - 3[\mathcal{K}][\mathcal{K}^2] + 2[\mathcal{K}^3], \\ \mathcal{U}_4 &\equiv [\mathcal{K}]^4 - 6[\mathcal{K}]^2[\mathcal{K}^2] + 8[\mathcal{K}][\mathcal{K}^3] + 3[\mathcal{K}^2]^2 - 6[\mathcal{K}^4], \end{aligned} \quad (2.2)$$

¹We set the Newtons gravitational constant G and the speed of light c to be $G = c = 1$.

in which

$$\mathcal{K}^\mu{}_\nu = \delta^\mu{}_\nu - \sqrt{g^{\mu\sigma} f_{ab} \partial_\sigma \Phi^a \partial_\nu \Phi^b},$$

where f_{ab} is a reference metric, while, $[\mathcal{K}] = \mathcal{K}^\mu{}_\mu$ and $[\mathcal{K}^n] = (\mathcal{K}^n)^\mu{}_\mu$ denote the traces. Here Φ^a are the Stückelberg scalars introduced to preserve the general covariance of the theory.

The above action admits static and spherically symmetric black hole solutions with the line element and reference metric, given respectively as:

$$ds^2 = -f(r)dt^2 + \frac{dr^2}{f(r)} + r^2(d\theta^2 + \sin^2\theta d\varphi^2), \quad (2.3)$$

$$f_{\mu\nu} = \text{diag}(0, 0, h^2, h^2 \sin^2\theta), \quad (2.4)$$

where h is a positive constant. Using an ansatz for the gauge potential $A_\mu = (A(r), 0, 0, 0)$, the lapse function $f(r)$ can be obtained to be

$$f(r) = 1 - \frac{2M}{r} + \frac{Q^2}{r^2} + \frac{\Lambda}{3}r^2 + \gamma r + \zeta, \quad (2.5)$$

where M is the mass and Q is the charge of the black hole, and the other parameters are defined as

$$\begin{aligned} \Lambda &= 3m_g^2(1 + \alpha + \beta), \\ \gamma &= -hm_g^2(1 + 2\alpha + 3\beta), \\ \zeta &= h^2m_g^2(\alpha + 3\beta). \end{aligned} \quad (2.6)$$

It was noted in [111] that, in certain parameter space of (α, β) , the charged (neutral) black hole can have at most four (three) event horizons. The asymptotic structure of the solution is determined by the signs of Λ and γ . The parameter Λ plays the role of cosmological constant. In the absence of graviton mass ($m_g = 0$), one can recover the standard Reissner-Nordstrom black hole solution. It should be mentioned that for a suitable choice of parameters (α, β) , and a reference metric, one can have de-Sitter/anti-de Sitter solutions, together with global monopole solutions. For further details regarding the possible space of solutions, one can refer [111].

3 Phase portraits and circular orbits of massive and massless particles

In this section, we aim to classify the trajectories of massless as well as massive test particles around neutral and charged black holes of massive gravity and, subsequently, study related phase portraits. Owing to the fact that the geometry has too many free parameters, namely, $M, Q, m_g, h, \alpha, \beta$, a comprehensive study of phase portraits will be beyond the scope of this section. In what follows, we fix M, Q, m_g and h and vary α, β . The ranges are chosen appropriately to capture distinct trajectories of the test particles.

We start with the geodesic equation for the line element (2.3), that is

$$\epsilon = -g_{\mu\nu} \dot{x}^\mu \dot{x}^\nu, \quad (3.1)$$

where the dot denotes a derivative with respect to an affine parameter which we will call τ , and ϵ takes values 1(0), for massive (massless) test particles. Considering the equatorial geodesics with $\theta = \pi/2$, and employing the conserved quantities associated with the symmetries of the spacetime (i.e., the energy $E = -g_{tt}\dot{t}$, and the orbital angular momentum $L = g_{\varphi\varphi}\dot{\varphi}$ of the test particle ²), the above geodesic equation reduces to

$$\dot{r}^2 + V_{\text{eff}} = 0, \quad (3.2)$$

where the effective potential V_{eff} is,

$$V_{\text{eff}} = f(r) \left(\frac{L^2}{r^2} + \epsilon \right) - E^2. \quad (3.3)$$

In the next two subsections, we examine (3.2), first for the photon around neutral and charged black hole, and then repeat the same exercise for a massive particle.

3.1 Fixed points and phase portraits for massless particle

To study photon trajectories around a neutral black hole, we start with explicit form of (3.2),

$$\dot{r}^2 = E^2 - \left(1 - \frac{2M}{r} + \frac{\Lambda}{3}r^2 + \gamma r + \zeta \right) \frac{L^2}{r^2}. \quad (3.4)$$

Since

$$\frac{d\phi}{d\tau} = \frac{L}{g_{\phi\phi}} = \frac{L}{r^2}, \quad (3.5)$$

we write

$$\begin{aligned} \left(\frac{dr}{d\phi} \right)^2 &= \left(\frac{dr}{d\tau} \right)^2 \left(\frac{d\tau}{d\phi} \right)^2 \\ &= \frac{r}{L^2} \left(E^2 r^3 - (r - 2M + \frac{\Lambda}{3}r^3 + \gamma r^2 + \zeta r) L^2 \right). \end{aligned} \quad (3.6)$$

It is useful to introduce a new variable $x = 1/r$. The governing equation now takes a simple form

$$\left(\frac{dx}{d\phi} \right)^2 = \frac{E^2}{L^2} - (x^2 - 2Mx^3 + \frac{\Lambda}{3} + \gamma x + \zeta x^2). \quad (3.7)$$

Differentiating once more, we get

$$\frac{d^2x}{d\phi^2} = -(1 + \zeta)x + 3Mx^2 - \frac{\gamma}{2}. \quad (3.8)$$

It is convenient to rewrite the above equation as a pair of first order differential equations

$$\begin{aligned} \frac{dx}{d\phi} &= z, \\ \frac{dz}{d\phi} &= -(1 + \zeta)x + 3Mx^2 - \frac{\gamma}{2}. \end{aligned} \quad (3.9)$$

²For massive test particle, E and L denote the conserved quantities per unit mass of the test particle.

The appearance of the phase portrait is controlled by the fixed points. These points are obtained by setting the right hand sides to zero. We get, therefore,

$$\begin{aligned} A : (z, x) &= \left(0, \frac{1}{6M}(1 + \zeta - \sqrt{1 + 6M\gamma + 2\zeta + \zeta^2})\right), \quad \text{and} \\ B : (z, x) &= \left(0, \frac{1}{6M}(1 + \zeta + \sqrt{1 + 6M\gamma + 2\zeta + \zeta^2})\right), \end{aligned} \quad (3.10)$$

as the two fixed points. Note that the reality condition implies

$$1 + 6M\gamma + 2\zeta + \zeta^2 \geq 0. \quad (3.11)$$

In terms of parameters (α, β) it takes the form

$$1 + 2h^2m_g^2(\alpha + 3\beta) + h^4m_g^4(\alpha + 3\beta)^2 - 6hMm_g^2(1 + 2\alpha + 3\beta) \geq 0. \quad (3.12)$$

Solving (3.10) and (3.7) simultaneously, we can easily find the energies associated with the fixed points in terms of M, L, γ and ζ .

Since we also require one or both the fixed points to lie outside the black hole horizon(s), additional constraints on the parameters appear. This is what we do next. Keeping M, m_g, h fixed and varying α, β , we look for the number of horizons as well as the fixed points outside the black hole. Our finding is summarised in Fig. (1).

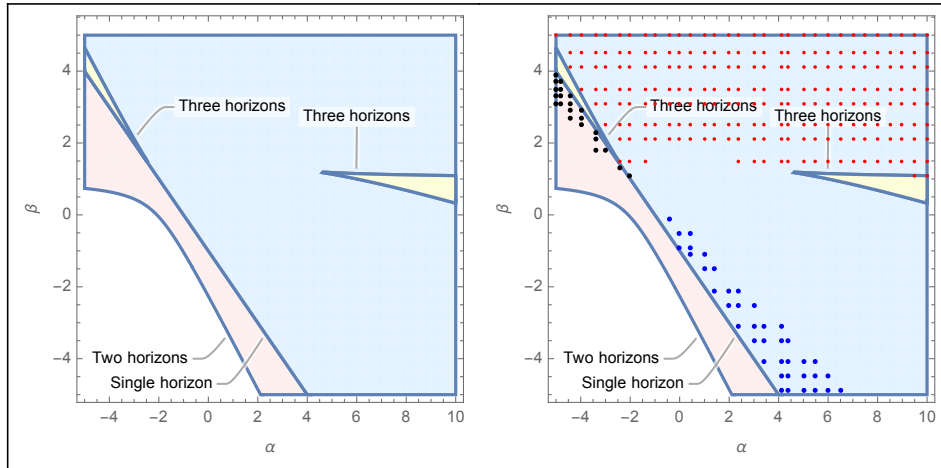


Figure 1: Left: Number of horizons as we vary α and β while keeping $M = m_g = h = 1, Q = 0$. There could be at most three horizons. Right: Locations and the nature of the fixed points are shown. Region marked with blue dots represents parameter values for which the fixed point B is outside the horizon. Similarly, for the one marked by the black dots, fixed point A is outside the outer horizon. Finally both A, B are both outside in the region marked by the red dots. For other regions with no dots, either fixed points are not real or lie behind the outer horizon. These plots are consistent with the constraint given in (3.12).

Natures of the fixed points are encoded in the Jacobian matrix following from (3.9). This is given by

$$J = \begin{bmatrix} \frac{\partial x'}{\partial x} & \frac{\partial x'}{\partial z} \\ \frac{\partial z'}{\partial x} & \frac{\partial z'}{\partial z} \end{bmatrix} = \begin{bmatrix} 0 & 1 \\ -(1 + \zeta) + 6Mx & 0 \end{bmatrix}. \quad (3.13)$$

Evaluating at the fixed points A or B gives

$$J = \begin{bmatrix} 0 & 1 \\ \mp \sqrt{1 + 6M\gamma + 2\zeta + \zeta^2} & 0 \end{bmatrix}, \quad (3.14)$$

respectively. Eigen values of this matrix determine the nature of the orbits. These are given by

$$\begin{aligned} \text{at } A : & \pm i(1 + 6M\gamma + 2\zeta + \zeta^2)^{\frac{1}{4}} \\ \text{at } B : & \pm (1 + 6M\gamma + 2\zeta + \zeta^2)^{\frac{1}{4}}. \end{aligned} \quad (3.15)$$

While purely imaginary values (as the quantity under fourth root is positive (3.11)) indicate that A is a center, B produces a saddle point. The complete phase portraits are obtained then by integrating (3.9) and shown in Fig. (2).

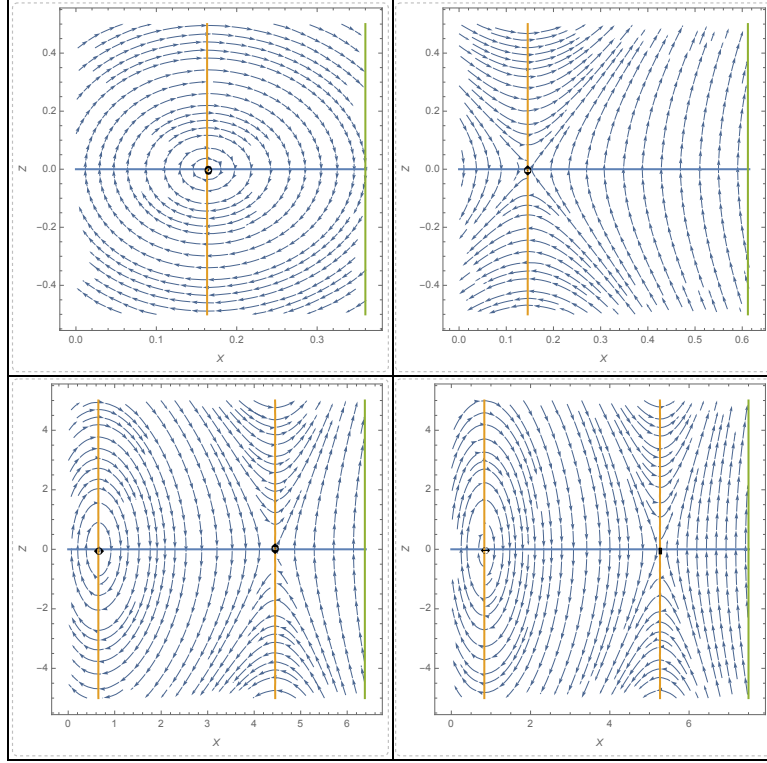


Figure 2: The figures show the phase plane portraits of massless particle outside an uncharged black hole. We vary (α, β) and keep $M = h = m_g = 1, Q = 0$. Top left: the fixed point outside the horizon is a center producing closed orbits. We have chosen $(\alpha, \beta) = (-4, 2.9)$. This point lies in the black-dotted region in Fig. (1). Top right: the fixed point now is a saddle which lies in the blue-dotted region of Fig.(1). We have taken $(\alpha, \beta) = (2, -2)$. Bottom row: these are for $(\alpha, \beta) = (2, 4.1)$ (left) and $(8, 3.1)$ (right), chosen from the red-dotted region of Fig. (1). In this region, both the fixed points are outside with the saddle being nearer to the horizon. In all these figures, the vertical lines drawn at extreme right represent the location of the outer horizon.

Now we move to the charged black hole. Except that the charge parameter makes the computation a bit messy, the analysis is same as before. We would therefore keep our discussion brief. The phase-plane equations now become

$$\begin{aligned} \frac{dx}{d\phi} &= z, \\ \frac{dz}{d\phi} &= -(1 + \zeta)x + 3Mx^2 - 2Q^2x^3 - \frac{\gamma}{2}. \end{aligned} \quad (3.16)$$

The fixed points are represented by the solutions of

$$z = 0, \text{ and } -(1 + \zeta)x + 3Mx^2 - 2Q^2x^3 - \frac{\gamma}{2} = 0. \quad (3.17)$$

The second equation could have at most three positive roots, providing us at most three fixed points. We also require to find the fixed points that lie outside the outer most horizon. Both are shown in Fig. (3).

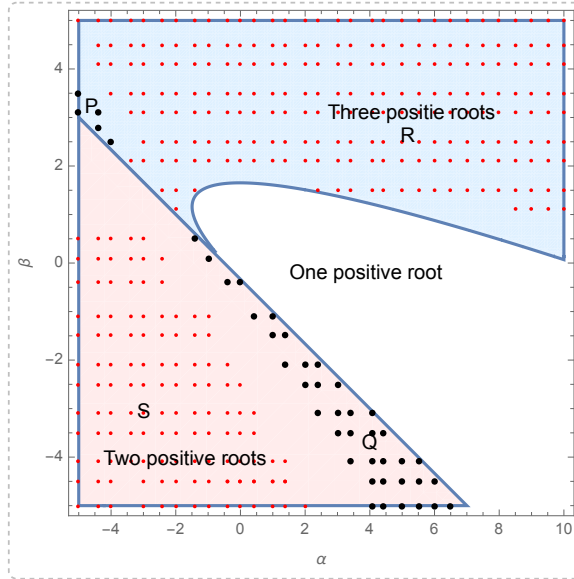


Figure 3: Number of positive roots of the right equation of (3.17) are shown in the (α, β) plane using three distinct colours. Further, the regions with black dots (P and Q) hold only one of the fixed points outside the outer horizon. While in region P , the node is a center, a saddle appears at Q . Two fixed points are located outside the outer horizon in the other two dotted regions (R and S). In R , the saddle node is closer to the horizon and in S , the center. In the rest of the parameter space, either no fixed point arises outside the outer horizon or they are complex. We have set $M = h = m_g = 1$, and $Q = .2$.

We now proceed to examine the nature of these fixed points. It is best done by linearising the system of equations around a fixed point $(z_0 = 0, x_0)$, where $x = x_0$ is a solution of the second equation of (3.17); to leading order, we get from (3.16),

$$\begin{aligned} \frac{d\delta x}{d\phi} &= \delta z, \\ \frac{d\delta z}{d\phi} &= -(1 - 6Mx_0 + 6Q^2x_0^2 + \zeta)\delta x. \end{aligned} \quad (3.18)$$

Here δz and δx represent small disturbances around the fixed point. The Jacobian matrix is then computed as

$$J = \begin{bmatrix} 0 & 1 \\ -(1 - 6Mx_0 + 6Q^2x_0^2 + \zeta) & 0 \end{bmatrix} \quad (3.19)$$

The eigenvalues of J are

$$\lambda_{\pm} = \pm \sqrt{-1 + 6Mx_0 - 6Q^2x_0^2 - \zeta}. \quad (3.20)$$

The eigen values depend on α, β (through x_0 and ζ) and also on M, Q . Clearly, there are two possibilities for λ_{\pm} . Either both are real, differing only by the sign in front, or, both are purely imaginary, equal in magnitude and opposite in sign. First fixed point represents a saddle and the other is that of a center. Having gotten the possible nature of the fixed points from the local analysis, we numerically find the complete phase portrait. As we vary α, β keeping rest of the

parameters fixed, we see either a single (saddle or center) or both (a saddle and a center) may appear outside the outer horizon. In fact, two fixed points, that is the center and the saddle could swap their positions outside the horizon as we vary the parameters. The details of the portraits are discussion in Fig. (4).

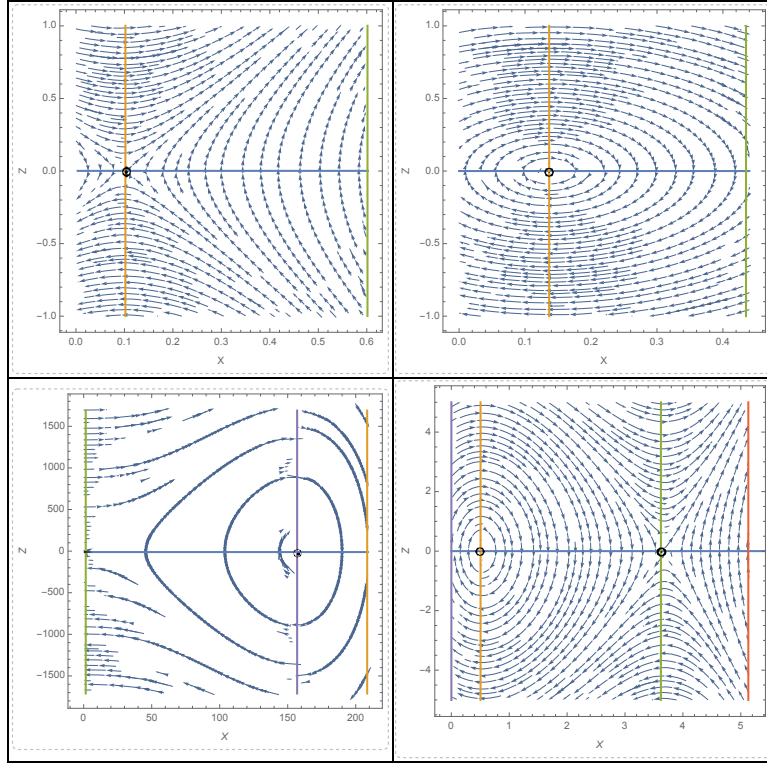


Figure 4: These figures show the phase plane portraits of massless particle outside a charged black hole as we vary (α, β) keeping $M = h = m_g = 1$ and $Q = 0.2$. Top left: The fixed point outside the horizon is a saddle with $\lambda_{\pm} = \pm 2.625$ for $(\alpha, \beta) = (5, -4.1)$. This is chosen from the region Q of figure (3). Top right: the node is now a center with $\lambda_{\pm} = \pm 2.254i$. The values of $(\alpha, \beta) = (-4.4, 3.1)$ lie in P of figure (3). Bottom left: it is for $(\alpha, \beta) = (-4, -4.1)$. While the node closer to the horizon is a center with $\lambda_{\pm} = \pm 22.56i$, the other one is a saddle with $\lambda_{\pm} = \pm 4.32$. This illustrates the region R of figure (3). Bottom right: Here $(\alpha, \beta) = (-1, 4.1)$. Nearer one to the horizon is now a saddle point with $\lambda_{\pm} = \pm 1.63$, and the one further away is a center, with $\lambda_{\pm} = \pm 3.05i$. This is typical of region S of figure (3). As we enter region S from R , we see the locations of the center and the saddle are swapped.

3.2 Fixed points and phase portraits for massive particle

While working with massive particles, two changes occur in the geodesic equation (3.3). First is that ϵ now takes the value one and the dependence of L , the angular momentum per unit mass, gets retained. In what follows, we will fix a representative value of L and obtain the phase portraits.

For a neutral black hole, massive particle follows

$$\dot{r}^2 + \left(1 - \frac{2M}{r} + \frac{\Lambda}{3}r^2 + \gamma r + \zeta\right) \left(\frac{L^2}{r^2} + 1\right) - E^2 = 0. \quad (3.21)$$

This can be brought to the form

$$\begin{aligned}\frac{dx}{d\phi} &= z, \\ \frac{dz}{d\phi} &= -(1 + \zeta)x + 3Mx^2 - \frac{\gamma}{2} + \frac{1}{L^2} \left(M + \frac{\Lambda}{3x^3} + \frac{\gamma}{2x^2} \right).\end{aligned}\quad (3.22)$$

We take $(z = 0, x = x_0)$ as a fixed point solution. To find the nature of this node, we linearise the above equations to get

$$\begin{aligned}\frac{d\delta x}{d\phi} &= \delta z, \\ \frac{d\delta z}{d\phi} &= \left(-1 - \alpha - 3\beta + 6Mx_0 + \frac{x_0(1 + 2\alpha + 3\beta) - 3(1 + \alpha + \beta)}{L^2x_0^4} \right) \delta x.\end{aligned}$$

The eigenvalues of the Jacobian matrix are then

$$\lambda_{\pm} = \pm \frac{1}{Lx_0^2} \sqrt{-3(1 + \alpha + \beta) + x_0(1 + 2\alpha + 3\beta) - L^2x_0^4(1 + \alpha + 3\beta) + 6L^2Mx_0^5}.\quad (3.23)$$

Since under the square root all the quantities are real, λ_{\pm} could be either real or purely imaginary numbers. Therefore, the nodes are either saddle point or center. We also require the nodes to be outside the outer horizon of the black hole. In the following, we set fixed values of M, L and study (3.24) numerically to arrive at the phases portraits. This is shown in figure (5).

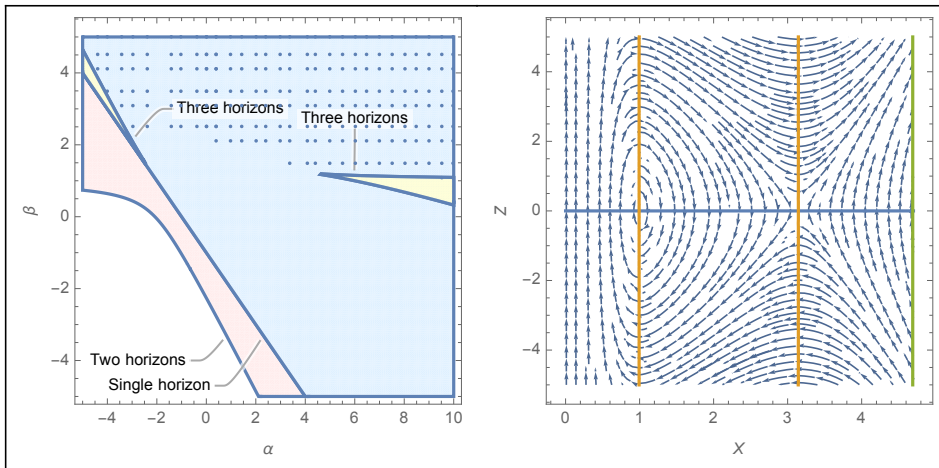


Figure 5: These figures show the nodes and corresponding phase portrait for a massive particle around an uncharged black hole for $M = 1, L = .5, m_g = h = 1, Q = 0$. Left: Dotted region represents the values of α, β for which nodes (one center and a saddle) appear outside the horizon. We also note that for these values of the parameters, the black hole possesses only a single horizon. Right: phase portrait, representing the center and the saddle outside the horizon (shown by the extreme right vertical line). This is drawn for $\alpha = 4.1, \beta = 2.5$.

Finally we examine the allowed trajectories of a massive particle around a charged black hole. The analogue of (3.22) are

$$\begin{aligned}\frac{dx}{d\phi} &= z, \\ \frac{dz}{d\phi} &= -(1 + \zeta)x + 3Mx^2 - 2Q^2x^3 - \frac{\gamma}{2} + \frac{1}{L^2} \left(M + \frac{\Lambda}{3x^3} - Q^2x + \frac{\gamma}{2} \right).\end{aligned}\quad (3.24)$$

Expanding around a fixed point ($z = 0, x = x_0$), where x_0 is a solution of the equation $dz/d\phi = 0$, we find the eigen values of the Jacobian matrix as

$$\lambda_{\pm} = \pm \frac{1}{Lx_0^2} \left[-3(1 + \alpha + \beta) + x_0(1 + 2\alpha + 3\beta) - L^2x_0^4(1 + \alpha + 3\beta) + 6L^2Mx_0^5 - Q^2x_0^4 - 6L^2Q^2x_0^6 \right]^{\frac{1}{2}}. \quad (3.25)$$

As earlier, these eigen values could either be real or purely imaginary. Hence the nodes could be either centers or saddle points. With these inputs coming from the local analysis, we find the phase portraits numerically. Figure (6) provides the trajectories emanating from (3.24).

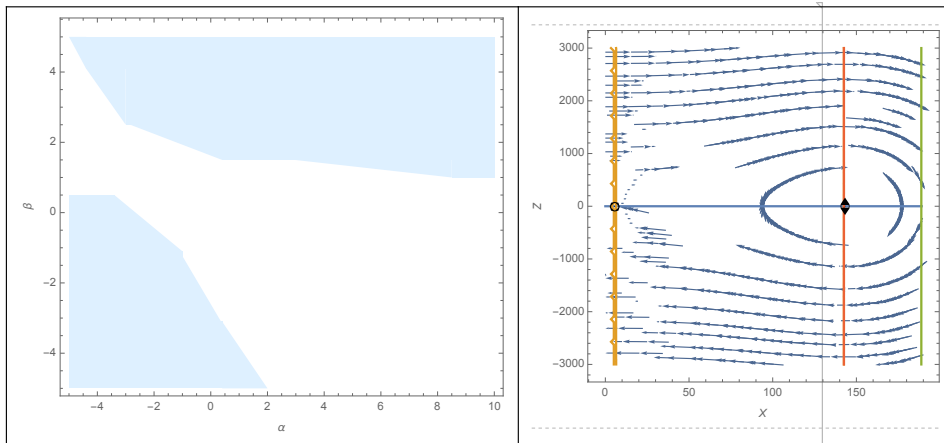


Figure 6: These figures show representative phase plane portrait of massive particle outside a charged black hole for $M = 1, Q = .2, L = .5, m_g = h = 1$. Left: A pair of nodes appear outside the outer horizon in the blue region – one is a saddle and the other being a center. Right: Typical portrait for $\alpha = 8, \beta = 4.1$. Nodes are marked with black dots. The vertical line on the right is the location of the outer horizon.

4 Static spheres

Having obtained the phase portraits of massive as well as massless particles around the neutral and the charged black holes in massive gravity, in this section, we specialise on the circular orbits of a massive particle. In particular, we focus on the static spheres – these are the circular orbits with vanishing orbital angular momentum [29]. The associated angular velocity of a particle executing such a trajectory, measured by a distant static observer, vanishes since

$$\Omega = \frac{\dot{\phi}}{\dot{t}} = \frac{f(r)L}{r^2E}. \quad (4.1)$$

4.1 Existence of static spheres

It is instructive to first have a look at the effective potential (3.3) as much can be understood from it. It reads, after setting $L = 0$,

$$V_{\text{eff}} = f(r) - E^2. \quad (4.2)$$

Further, the conditions for the circular orbits to occur are $V_{\text{eff}} = V'_{\text{eff}} = 0$, where prime denotes derivative with respect to r . These two equations together give the energy and the radius (r_{sp})

of the static sphere as

$$E = \sqrt{f(r_{\text{sp}})}, \quad (4.3)$$

$$f'(r_{\text{sp}}) = 0. \quad (4.4)$$

For the above conditions to make sense, the lapse function $f(r)$ needs to be positive, and should necessarily have extremal points. For the present case, there exist a wide range of parameter values, for which the lapse function $f(r)$, given in (2.5), fulfils all the requirements. For brevity, we directly present the behaviour of $f(r)$ in Fig. (7) for some choices of parameters.

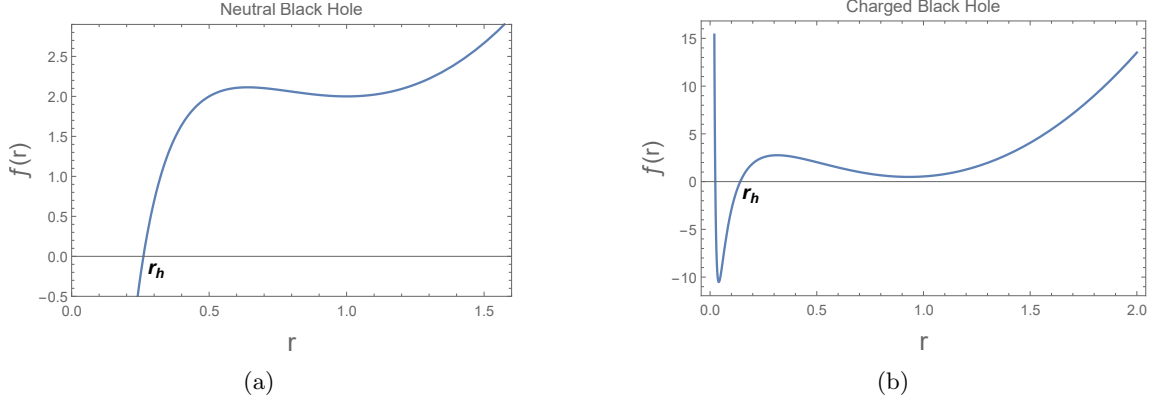


Figure 7: Behavior of the lapse function $f(r)$. (a) for a neutral black hole with single horizon at $r_h = 0.2610$ (here, we set $M = m_g = h = 1, Q = 0, \alpha = 0, \beta = 3$). (b) for a charged black hole with two horizons (inner and outer) where the outer horizon is located at $r_h = 0.1414$ (here, we set $M = m_g = h = 1, Q = 0.2, \alpha = 10, \beta = 1.5$).

Further, the effective potential (4.2) plotted in Fig. (8) for both neutral and charged black holes, shows the existence of one stable and one unstable static sphere at r_{sp1} and r_{sp2} , for fixed energy E_{sp1} and E_{sp2} , respectively.

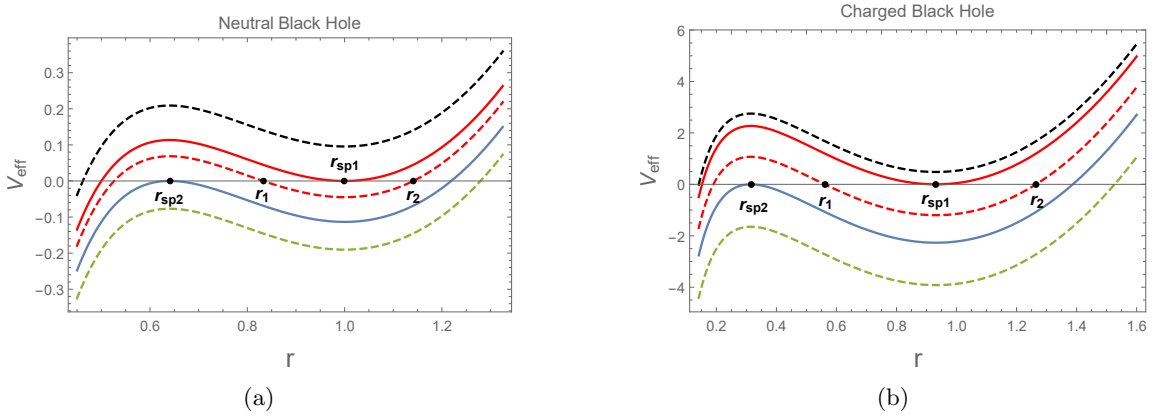


Figure 8: Behavior of the effective potential (4.2) for various energies E , of the massive test particle. (a) for neutral black hole background (here, we set $M = m_g = h = 1, Q = 0, \alpha = 0, \beta = 3$). $E = 1.38, 1.414 (E_{\text{sp1}}), 1.43, 1.454 (E_{\text{sp2}}), 1.48$ from top to bottom. The stable static sphere is located at $r_{\text{sp1}} = 1$, while the unstable static sphere is located at $r_{\text{sp2}} = 0.6404$. (b) for charged black hole background (here, we set $M = m_g = h = 1, Q = 0.2, \alpha = 10, \beta = 1.5$). $E = 0.1, 0.7014 (E_{\text{sp1}}), 1.3, 1.66185 (E_{\text{sp2}}), 2.1$ from top to bottom. The stable static sphere is located at $r_{\text{sp1}} = 0.93182$, while the unstable static sphere is located at $r_{\text{sp2}} = 0.3146$.

The motion of the massive test particle, possessing the energy $E \in (E_{\text{sp1}}, E_{\text{sp2}})$, will be bounded between the two turning points r_1 and r_2 of the potential, see the Fig. (8). This is a straight back-and-forth motion between r_1 and r_2 , as there is no angular motion, on account of vanishing angular velocity. From the radial motion, plotted in $r - t$ plane in Fig. (12), one can see that the radial distance of the motion between r_1 and r_2 narrows as the energy E decreases. In fact, when $E = E_{\text{sp1}}$, we see that $r_1 = r_2 = r_{\text{sp1}}$. Thus, the radial distance remains unchanged with the coordinate time, indicating that there is a static sphere at $r = r_{\text{sp1}}$.

Further insights into the nature of the static spheres can be gained from a direct study of the dynamical equation that follows from (3.2). To this end, we differentiate this equation to get

$$\ddot{r} = \frac{1}{6r^3} \left(-6Mr + 6Q^2 - 2\Lambda r^4 - 3\gamma r^3 \right). \quad (4.5)$$

It is convenient to convert this to a set of two first order differential equations as

$$\begin{aligned} \dot{r} &= z, \\ \dot{z} &= \frac{1}{6r^3} \left(-6Mr + 6Q^2 - 2\Lambda r^4 - 3\gamma r^3 \right). \end{aligned} \quad (4.6)$$

Fixed points are obtained by setting $\dot{r} = \dot{z} = 0$. These conditions are equivalent to equating $V_{\text{eff}} = V'_{\text{eff}} = 0$. Figures (9) and (10) describes our results that we obtained numerically analysing equations (4.6) around neutral and charged black holes, respectively.

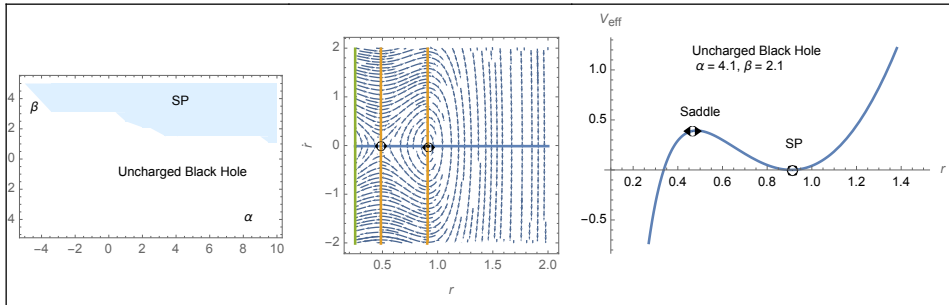


Figure 9: Static spheres around an uncharged black hole. We have set $M = m_g = h = 1, Q = 0$. Left: Region in blue shows the values of α, β for which static spheres appear. Ranges of α, β are chosen only for the representative purpose. Middle: Fixed points, denoted in black, and the vector fields around those are shown. The chosen values of (α, β) are $(4.1, 2.1)$. The vertical line on the extreme left is the location of the outer horizon. Right: Shape of the effective potential following from (4.2) for $(\alpha, \beta) = (4.1, 2.1)$. The energy associated with the particle is $E = 1.03$.

4.2 Number of static spheres

We have seen in the previous subsection that, for both neutral and charged black holes, there exists one pair of static spheres (stable and unstable), where we handpicked certain values of massive gravity parameters and used them in the lapse function $f(r)$, in eqn. (2.5). However, for arbitrary values of massive gravity parameters, it is important to know, under what conditions in the region outside the black hole (neutral or charged), do the static spheres exist. This question can be answered by studying the topological properties of the static spheres, which can exist for the lapse function in eqn. (2.5), following [29].

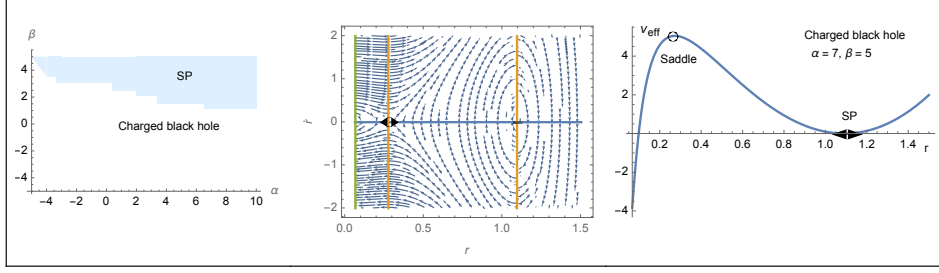


Figure 10: Static spheres around a charged black hole. We have set $M = m_g = h = 1$ and $Q = .2$. Left: Regions in blue show the values of α, β for which static spheres occur. Ranges of α, β are chosen only for the representative purpose. Middle: Fixed points, denoted in black, and the vector fields around those are shown. The chosen values of (α, β) are $(7, 5)$. Shape of the effective potential following from (4.2) for $\alpha = 7$ and $\beta = 5$. The energy associated with the particle is $E = 1.98$.

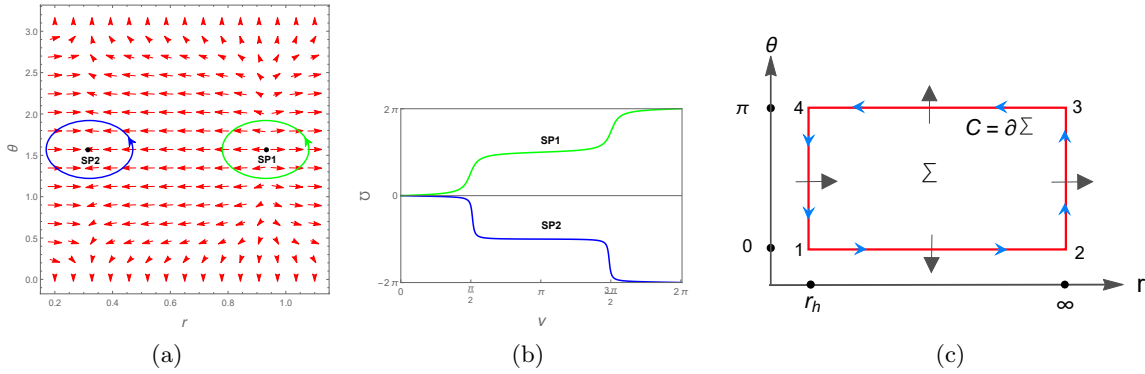


Figure 11: (a) The normalised vector field n , in $\theta - r$ plane, vanishing at the stable (SP1) and unstable (SP2) static spheres. (b) The deflection angle $\mathcal{U}(v)$ of the vector field ϕ , giving the winding number $+1$ for stable (SP1) static sphere, and -1 for unstable (SP2) static sphere. Here, plots (a) and (b) are shown for charged black hole case (similar results can be deduced for neutral black hole case, which we do not show). Here, we set $M = m_g = h = 1, Q = 0.2, \alpha = 10, \beta = 1.5$. (c) The rectangular contour C denotes the entire boundary of the parameter space Σ . The black arrows show the direction of the vector field ϕ along the boundary.

Using the lapse function $f(r)$, we define a vector field $\phi(\phi^r, \phi^\theta)$ as [29]:

$$\phi^r = \frac{\partial f(r)}{\partial r}, \quad \phi^\theta = -\frac{\cos\theta}{\sin^2\theta}. \quad (4.7)$$

This vector field ϕ vanishes exactly at the location of static spheres. One can assign a topological charge (i.e., winding number w) for each static sphere by defining a topological current j^μ , which is identically conserved, i.e., $\partial_\mu j^\mu = 0$, given by [29]:

$$j^\mu = \frac{1}{2\pi} \epsilon^{\mu\nu\rho} \epsilon_{ab} \partial_\nu n^a \partial_\rho n^b, \quad \mu, \nu, \rho = 0, 1, 2, \text{ and } a, b = 1, 2, \quad (4.8)$$

where $n = (\frac{\phi^r}{\|\phi\|}, \frac{\phi^\theta}{\|\phi\|})$ is the normalized vector field. A stable static sphere possesses the winding number $+1$, whereas for an unstable static sphere it is -1 (see Fig. 11a and Fig. 11b).

We, now compute the total winding number W , which is the sum of the winding numbers of all the static spheres existing in the entire parameter space Σ outside the horizon. For this, consider a closed rectangular contour C , which is piece-wise smooth and positive oriented, that encloses the entire parameter space Σ , as shown in Fig. 11c. Then, the computation of the

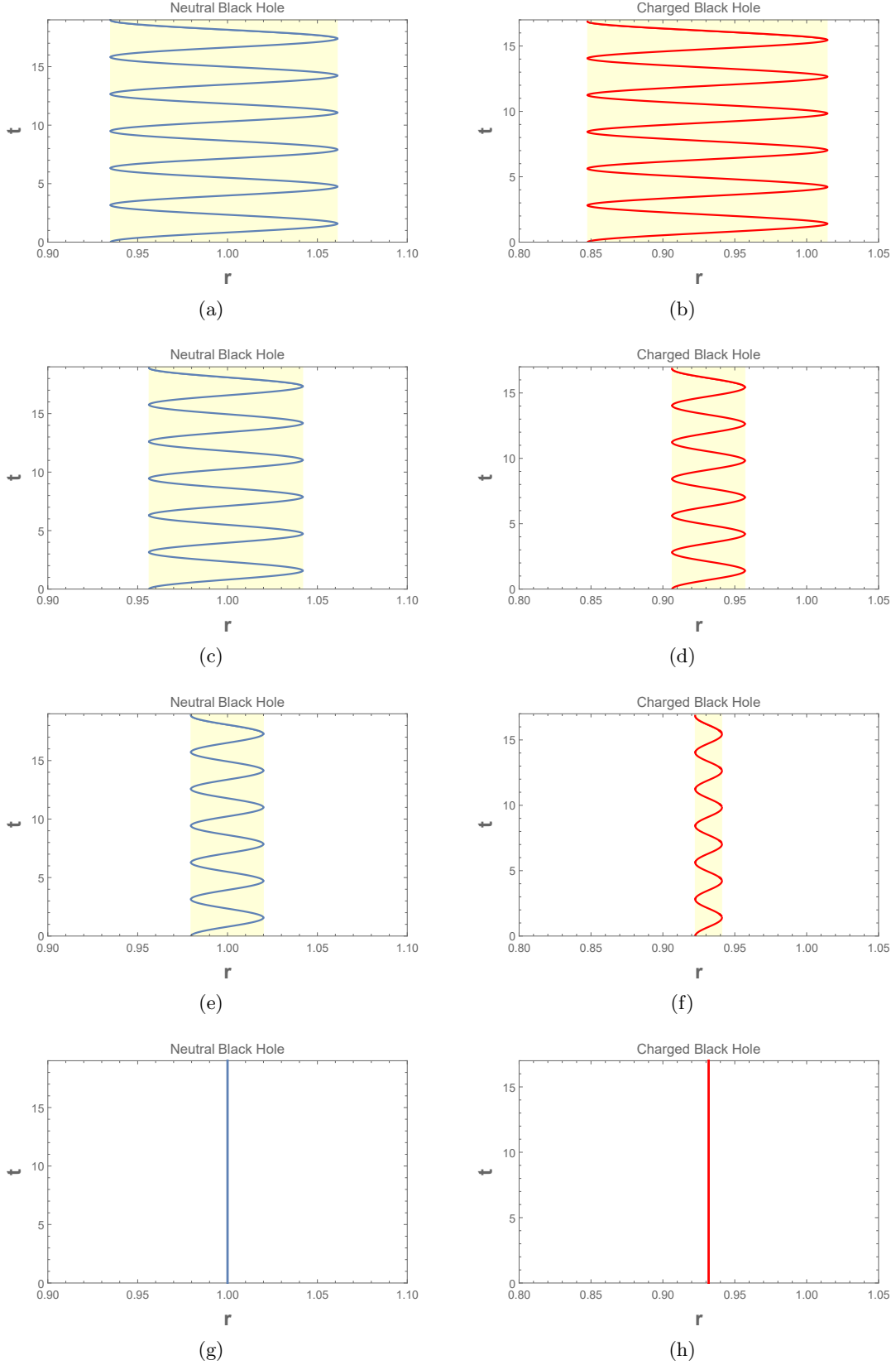


Figure 12: Radial motion of the massive test particle. Left panel for neutral black hole background (here, we set $M = m_g = h = 1, Q = 0, \alpha = 0, \beta = 3$). (a) $E = 1.4170$, (c) $E = 1.4155$, (e) $E = 1.4145$, and (g) $E = E_{sp1} = 1.414$. Right panel for charged black hole background (here, we set $M = m_g = h = 1, Q = 0.2, \alpha = 10, \beta = 1.5$). (b) $E = 0.75$, (d) $E = 0.706$, (f) $E = 0.702$, and (h) $E = E_{sp1} = 0.7014$. When $E = E_{sp1}$, the radial motion is just a horizontal line denoting a static orbit with vanishing angular momentum.

deflection \mathcal{U} of the vector field ϕ along the contour C , gives the total winding number within C as:

$$W = \sum_i w_i = \frac{1}{2\pi} \oint_C d\mathcal{U}, \quad (4.9)$$

where we define,

$$\phi^r = \|\phi\| \cos\mathcal{U}, \quad (4.10)$$

$$\phi^\theta = \|\phi\| \sin\mathcal{U}. \quad (4.11)$$

We can write the integration in eqn. (4.9) as

$$\frac{1}{2\pi} \oint_C d\mathcal{U} = \frac{1}{2\pi} \left(\int_{r_h}^{\infty} d\mathcal{U} \Big|_{\theta=0} + \int_0^{\pi} d\mathcal{U} \Big|_{r=\infty} + \int_{\infty}^{r_h} d\mathcal{U} \Big|_{\theta=\pi} + \int_{\pi}^0 d\mathcal{U} \Big|_{r=r_h} \right), \quad (4.12)$$

which can be computed as follows [25, 29]:

At $\theta = 0, \pi$.

We have, from eqn. (4.11), $\mathcal{U} = \arcsin\left(\frac{\phi^\theta}{\|\phi\|}\right)$, which becomes

$$\mathcal{U}|_{\theta=0,\pi} = \arcsin\left(\frac{\phi^\theta}{\|\phi\|}\right) = \begin{cases} \arcsin(-1) = -\frac{\pi}{2}, & \text{for } \theta = 0. \\ \arcsin(+1) = +\frac{\pi}{2}, & \text{for } \theta = \pi. \end{cases} \quad (4.13)$$

This shows that the direction of the vector field ϕ is downwards at $\theta = 0$, and upwards at $\theta = \pi$. Further, we get $\int_{r_h}^{\infty} d\mathcal{U} \Big|_{\theta=0} = \int_{\infty}^{r_h} d\mathcal{U} \Big|_{\theta=\pi} = 0$ (as $d\mathcal{U}|_{\theta=0,\pi} = 0$).

At $r = r_h$.

For the lapse function eqn. (2.5), we have $f(r_h) = 0$ at horizon r_h , and in order for the static spheres to exist, one should have $f(r > r_h) > 0$. Near the horizon, this implies $\frac{\partial f(r)}{\partial r} = \phi^r > 0$, indicating that the direction of the vector field ϕ at $r = r_h$, is rightward.

Since, the vector field ϕ is changing the direction from upwards (i.e., $\mathcal{U} = +\frac{\pi}{2}$) at $\theta = \pi$, to downwards (i.e., $\mathcal{U} = -\frac{\pi}{2}$) at $\theta = 0$, along the line segment 4 \rightarrow 1 of the contour C (in clock wise direction), we get

$$\int_{\pi}^0 d\mathcal{U} \Big|_{r=r_h} = \mathcal{U} \Big|_{\theta=0} - \mathcal{U} \Big|_{\theta=\pi} = -\frac{\pi}{2} - \frac{\pi}{2} = -\pi. \quad (4.14)$$

At $r = \infty$.

For the lapse function in eqn. (2.5), one can check that $f(r)$ at $r \rightarrow \infty$, obeying $f(r > r_h) > 0$, ensures that $\frac{\partial f(r)}{\partial r} = \phi^r$ is positive. Thus, the direction of the vector field ϕ at $r \rightarrow \infty$ is rightward.

Since, the vector field ϕ is changing direction from downwards (i.e., $\mathcal{U} = -\frac{\pi}{2}$) at $\theta = 0$, to upwards (i.e., $\mathcal{U} = +\frac{\pi}{2}$) at $\theta = \pi$, along the line segment 2 \rightarrow 3 of the contour C (in anti-clock

wise direction), we get

$$\int_0^\pi d\mathcal{U}\Big|_{r=\infty} = \mathcal{U}\Big|_{\theta=\pi} - \mathcal{U}\Big|_{\theta=0} = \frac{\pi}{2} + \frac{\pi}{2} = +\pi. \quad (4.15)$$

Therefore, we get the total winding number $W = \frac{1}{2\pi}(0 + \pi + 0 - \pi) = 0$. This shows that if static spheres exist, the stable and unstable static spheres always come in pairs.

4.3 Aschenbach effect

As noted earlier [113], the presence of static spheres and stable photon spheres around a static and spherically symmetric black hole may indicate the occurrence of a peculiar phenomenon called *Aschenbach effect*, where the angular velocity of a time-like circular orbit is found to be increasing with its radius coordinate.

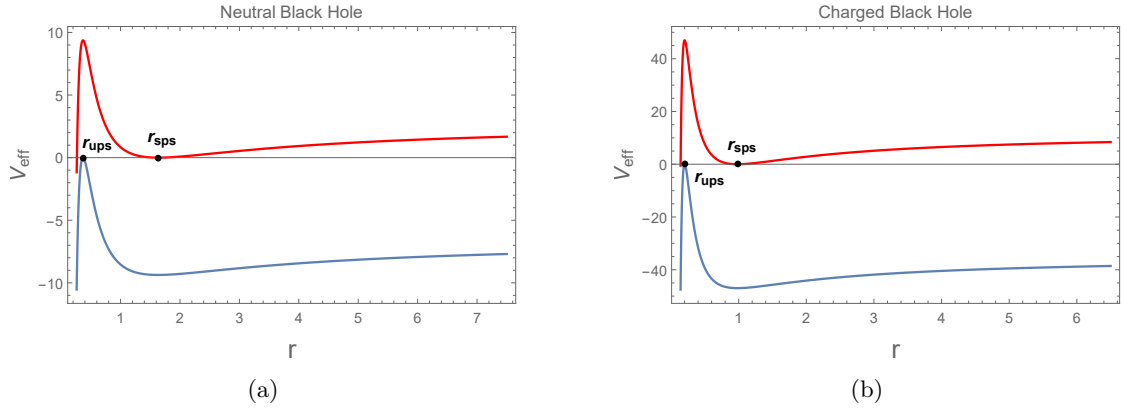


Figure 13: Plot of effective potential of a photon with fixed angular momentum L and for various energies E , showing the existence of stable photon sphere (sps) and unstable photon sphere (ups), outside the horizon. (a) for neutral black hole (where we set $M = m_g = h = 1, Q = 0, \alpha = 0, \beta = 3$). Red curve for $E = E_{\text{sps}} = 1.08028L$, and blue curve for $E = E_{\text{ups}} = 3.24603L$. $(r_{\text{sps}}, r_{\text{ups}}) = (1.632, 0.3675)$. (b) for charged black hole (where we set $M = m_g = h = 1, Q = 0.2, \alpha = 10, \beta = 1.5$). Red curve for $E = E_{\text{sps}} = 0.73281L$, and blue curve for $E = E_{\text{ups}} = 6.8925L$. $(r_{\text{sps}}, r_{\text{ups}}) = (0.982761, 0.201191)$. All plots are shown for $L = 1$.

Before looking for *Aschenbach effect*, the presence of static spheres around the black holes in massive gravity noted in the last subsection, motivates us to search also for the presence of stable photon spheres, which might be precursors for such an effect. For this, we write the effective potential (3.3) for photons (i.e., massless particles) as,

$$V_{\text{eff}} = f(r)\left(\frac{L^2}{r^2}\right) - E^2, \quad (4.16)$$

Its behaviour, for the case of fixed angular momentum $L \neq 0$ and for various energies E , can be seen in Fig. 13, for both neutral and charged black holes. We find that, for a given angular momentum L , there exist a pair of stable and unstable photon spheres for both neutral and charged black holes. These occur at $(r_{\text{sps}}, r_{\text{ups}}) = (1.632, 0.3675)$ for neutral black hole, and $(r_{\text{sps}}, r_{\text{ups}}) = (0.982761, 0.201191)$ for charged black hole.

Thus, due to the existence of one stable photon sphere outside the horizon of neutral and charged black holes, in what follows, we focus on the circular geodesics of a massive test particle ³ (i.e., timelike circular orbits (TCOs)) in order to examine the occurrence of *Aschenbach effect*.

The plot of effective potential (3.3) for a massive test particle is given in Fig. 14. We see that for a given angular momentum L , there exist a pair of stable and unstable TCOs, such that the stable one is the outer TCO and the unstable one is the inner TCO, which exist in both neutral and charged black hole backgrounds.

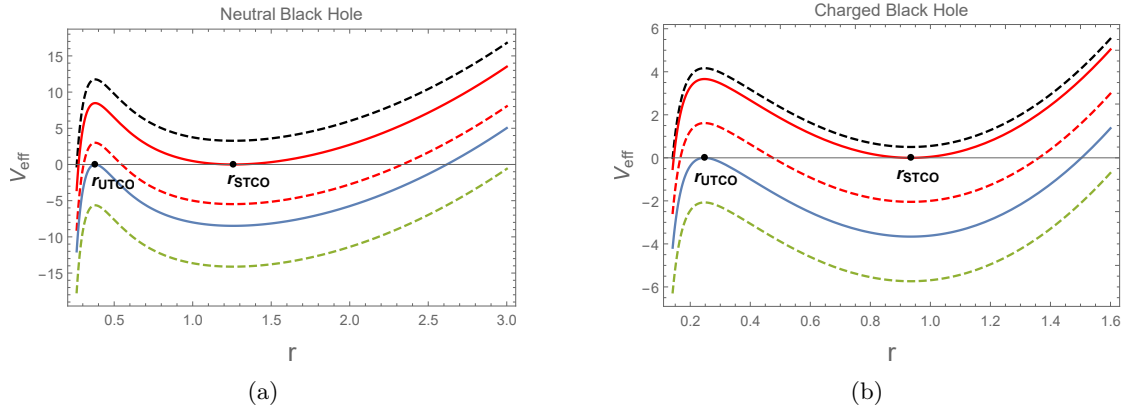


Figure 14: Plot of effective potential of a massive test particle having fixed angular momentum L and for various energies E , showing the existence of stable timelike circular orbit (STCO) and unstable timelike circular orbit (UTCO). (a) for neutral black hole: where, $M = m_g = h = 1, Q = 0, \alpha = 0, \beta = 3, L = 1$, and $E = 0.5, 1.87 (E_{STCO}), 3, 3.464 (E_{UTCO})$, and 4.2 from top to bottom. $(r_{STCO}, r_{UTCO}) = (1.258, 0.379)$. (b) for charged black hole: where, $M = m_g = h = 1, Q = 0.2, \alpha = 10, \beta = 1.5, L = 0.2$, and $E = 0.1, 0.7173 (E_{STCO}), 1.6, 2.0437 (E_{UTCO})$, and 2.5 from top to bottom. $(r_{STCO}, r_{UTCO}) = (0.9341, 0.2475)$.

One can obtain the expressions for the energy E and angular momentum L of a TCO, using $V_{\text{eff}} = 0$, and $V'_{\text{eff}} = 0$, given by [113]:

$$E = f \sqrt{\frac{2}{2f - rf'}}, \quad (4.17)$$

$$L = r^{3/2} \sqrt{\frac{f'}{2f - rf'}}. \quad (4.18)$$

The behaviour of E and L of time-like circular orbits, for both neutral and charged black holes in massive gravity theory is shown in Fig. 15. One can see that the angular momentum curve is disconnected in a certain region where it becomes imaginary, implying that the corresponding TCOs should be excluded. Therefore, the stable and unstable TCO regions are disconnected, where the inner most stable TCO (ISCO) is located at $r_{\text{ISCO}} = 1$ for neutral black hole, and $r_{\text{ISCO}} = 0.93182$ for charged black hole. We also note that, in both neutral and charged black hole backgrounds, the marginally stable TCO lies in the region corresponding to imaginary L , and thus it does not coincide with the ISCO. Further, we observe from Fig. 15, that both the energy and angular momentum of the TCO diverge at the location of photon spheres.

³See [112, 114] for some possible null and timelike trajectories for our system.

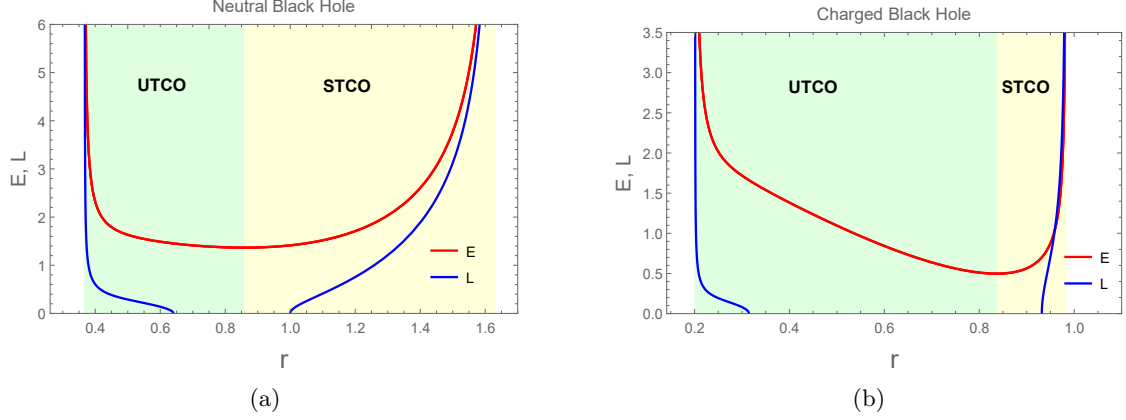


Figure 15: The energy E and the angular momentum L of the TCOs. The regions in light green and yellow colors are for the unstable TCO (UTCO) and stable TCO (STCO) regions, respectively. (a) for neutral black hole background (here, we set $M = m_g = h = 1, Q = 0, \alpha = 0, \beta = 3$). (b) for charged black hole background (here, we set $M = m_g = h = 1, Q = 0.2, \alpha = 10, \beta = 1.5$). The angular momentum curve is disconnected in the region where it takes imaginary values. E and L diverge at the location of photon spheres i.e., at $(r_{\text{sps}}, r_{\text{ups}}) = (1.632, 0.3675)$ for neutral black hole and at $(r_{\text{sps}}, r_{\text{ups}}) = (0.982761, 0.201191)$ for charged black hole.

Now, using the eqns. (4.1), (4.17) and (4.18), we compute the angular velocity Ω_{CO} of a TCO, measured by a static observer at rest, given by [113]:

$$\Omega_{\text{CO}} = \sqrt{\frac{f'}{2r}}, \quad (4.19)$$

where, its behaviour can be seen in Fig. 16. One immediately notes that, only in the stable TCO region, the angular velocity Ω_{CO} increases with the radius of the TCO. Moreover, this increasing behaviour of Ω_{CO} occurs near the stable photon sphere (SPS), and also Ω_{CO} maintains finite values at the location of photon spheres, as noted in [113]. Therefore, we confirm that the *Aschenbach effect* can be observed in both neutral and charged black hole backgrounds in massive gravity.

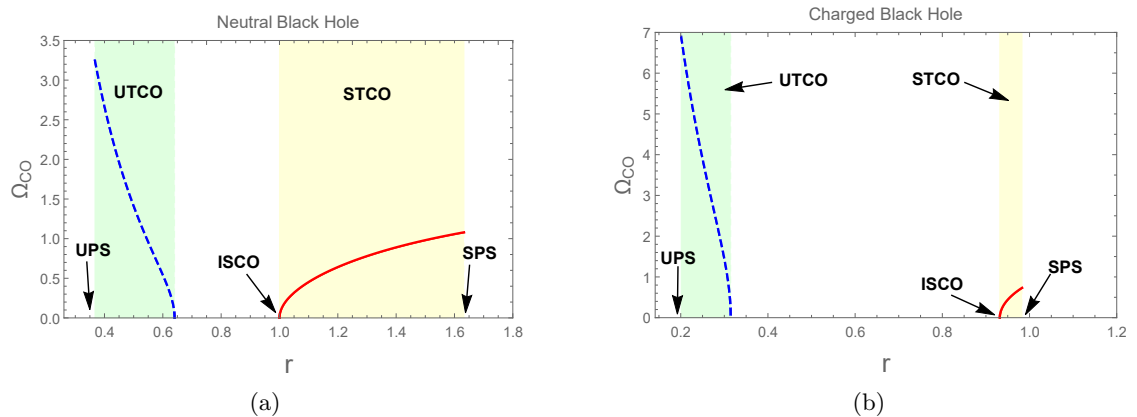


Figure 16: The orbital angular velocity profile Ω_{CO} of the TCOs. The regions in light green and yellow colors are for the unstable TCO (UTCO) and stable TCO (STCO) regions, respectively. “ISCO” denotes the innermost stable TCO. “UPS” and “SPS” denote the unstable and stable photon spheres. (a) for neutral black hole background, where we set $M = m_g = h = 1, Q = 0, \alpha = 0, \beta = 3$, and take $r_h = 0.2610, r_{\text{ups}} = 0.3675, r_{\text{ISCO}} = 1, r_{\text{sps}} = 1.632$. (b) for charged black hole background, where we set $M = m_g = h = 1, Q = 0.2, \alpha = 10, \beta = 1.5$, and take $r_h = 0.1414, r_{\text{ups}} = 0.201191, r_{\text{ISCO}} = 0.93182, r_{\text{sps}} = 0.982761$.

5 Conclusions

In this paper, we considered the 4-dimensional static and spherically symmetric black holes in dRGT massive gravity theory, where the charged (neutral) black holes can admit at most four (three) event horizons in certain parameter space (α, β) of the theory. In these static and spherically symmetric black hole backgrounds, we studied geodesics of massive and massless test particles with particular attention to the circular geodesics.

Owing to the structure of the black holes in the massive gravity, the particle trajectories around these black holes could be diverse in nature. Therefore, via a phase-plane analysis, we first examined the fixed points and the phase portraits of these particles. We found that the fixed points, that lie outside the outer horizon, are either centers or saddle-nodes or both. Consequently, the trajectories offer closed orbits, including the circular one. Subsequently, we focussed on the possible existence of circular orbits for a massive test particle when its orbital angular momentum vanishes. These type of circular orbits are called as static spheres, where one may realise the construction of a static Dyson-like sphere [29]. We found that a pair of stable and unstable static spheres exists in both neutral and charged black hole backgrounds. Making use of a topological argument for static spheres, we showed that, in a general static and spherically symmetric black hole (charged or neutral) background in massive gravity, the stable and unstable static spheres always come in pairs, if they exist. The stable and unstable static sphere possess the topological charge $+1$ and -1 , respectively. These topological classifications are found to be in agreement with the analysis done for a dyonic black hole in quasitopological electromagnetism [29].

Next, we searched for the existence of stable photon spheres. We observed that, for a given angular momentum L , there exists a pair of stable and unstable photon spheres in both neutral and charged black hole backgrounds. In [113], the presence of static spheres and stable photon spheres around a static and spherically symmetric black hole, signalled the occurrence of Aschenbach effect. Motivated by this, we focused on the properties of time-like circular orbits (TCOs) in order to see such effect in the massive gravity theory, with results distinct from Einstein gravity.

In the case of dyonic black hole in quasi-topological electromagnetism, there exist two pairs of TCOs for a given angular momentum [113]. In contrast, for the neutral and charged black hole backgrounds in massive gravity considered here, we found only one pair of stable and unstable TCOs, such that the stable one is the outer TCO, and the unstable one is the inner TCO. Moreover, it is observed that certain TCOs have imaginary angular momentum, due to which the stable and unstable TCO regions are disconnected.

We then proceeded by computing the angular velocity Ω_{CO} of the TCOs, measured by a static observer at rest. We found the monotonically increasing behaviour of Ω_{CO} with radius of the TCO, in the stable region of TCOs region, near the stable photon sphere. This then confirms the existence of Aschenbach effect for time-like particle motion around both neutral and charged black hole backgrounds in massive gravity.

Together with the dyonic black hole in quasi-topological electromagnetism [29, 113], the neutral and charged black hole backgrounds in massive gravity studied in this work are the other

examples for existence of static spheres and the Aschenbach effect as well.

It would be interesting to find other systems, that show these properties. Finding a general condition, possibly using the topological arguments, which could allow prediction of static spheres and Aschenbach effect, would be nice to explore. Checking the occurrence of Aschenbach effect with a charged test particle for our system and also for dyonic black hole in quasi-topological electromagnetism [113], in addition to studying the effect of charge of the black hole, are possible avenues for future work. Investigating static spheres and Aschenbach effect from AdS/CFT point of view, possibly using some recently developed techniques [115, 116], would likely result in novel holographic understanding. We leave these issues for future work.

Acknowledgements

We have benefitted from discussions with Chethan Gowdigere and Arindam Lala. CB is grateful to CERN, Geneva for financial support and hospitality through Strings 2024 fellowship. CB thanks Iosif Bena and Nick Warner for warm hospitality at IPhT, Saclay, where some part of this work was done, and Soumangsu Chakraborty for helpful discussions.

References

- [1] B. P. Abbott *et al.* (LIGO Scientific, Virgo), *Phys. Rev. Lett.* **116**, 061102 (2016), arXiv:1602.03837 [gr-qc] .
- [2] K. Akiyama *et al.* (Event Horizon Telescope), *Astrophys. J. Lett.* **930**, L12 (2022), arXiv:2311.08680 [astro-ph.HE] .
- [3] K. Akiyama *et al.* (Event Horizon Telescope), *Astrophys. J. Lett.* **875**, L1 (2019), arXiv:1906.11238 [astro-ph.GA] .
- [4] P. Grandclement, C. Somé, and E. Gourgoulhon, *Phys. Rev. D* **90**, 024068 (2014), arXiv:1405.4837 [gr-qc] .
- [5] M. Grould, Z. Meliani, F. H. Vincent, P. Grandclément, and E. Gourgoulhon, *Class. Quant. Grav.* **34**, 215007 (2017), arXiv:1709.05938 [astro-ph.HE] .
- [6] M. C. Teodoro, L. G. Collodel, and J. Kunz, *JCAP* **03**, 063 (2021), arXiv:2011.10288 [gr-qc] .
- [7] M. C. Teodoro, L. G. Collodel, D. Doneva, J. Kunz, P. Nedkova, and S. Yazadjiev, *Phys. Rev. D* **104**, 124047 (2021), arXiv:2108.08640 [gr-qc] .
- [8] G. W. Gibbons and C. A. R. Herdeiro, *Class. Quant. Grav.* **16**, 3619 (1999), arXiv:hep-th/9906098 .
- [9] C. A. R. Herdeiro, *Nucl. Phys. B* **582**, 363 (2000), arXiv:hep-th/0003063 .
- [10] V. Diemer and J. Kunz, *Phys. Rev. D* **89**, 084001 (2014), arXiv:1312.6540 [gr-qc] .
- [11] J. F. M. Delgado, C. A. R. Herdeiro, and E. Radu, *Phys. Rev. D* **105**, 064026 (2022), arXiv:2107.03404 [gr-qc] .

- [12] Z. Stuchlik and S. Hledik, *Phys. Rev. D* **60**, 044006 (1999).
- [13] J. Levin and G. Perez-Giz, *Phys. Rev. D* **77**, 103005 (2008), arXiv:0802.0459 [gr-qc] .
- [14] D. Pugliese, H. Quevedo, and R. Ruffini, *Phys. Rev. D* **83**, 024021 (2011), arXiv:1012.5411 [astro-ph.HE] .
- [15] E. Hackmann, C. Lammerzahl, V. Kagramanova, and J. Kunz, *Phys. Rev. D* **81**, 044020 (2010), arXiv:1009.6117 [gr-qc] .
- [16] J. R. Villanueva, J. Saavedra, M. Olivares, and N. Cruz, *Astrophys. Space Sci.* **344**, 437 (2013).
- [17] S.-W. Wei and Y.-X. Liu, *Phys. Rev. D* **97**, 104027 (2018), arXiv:1711.01522 [gr-qc] .
- [18] B. Chandrasekhar and S. Mohapatra, *Phys. Lett. B* **791**, 367 (2019), arXiv:1805.05088 [hep-th] .
- [19] A. Lehébel and V. Cardoso, *Phys. Rev. D* **105**, 064014 (2022), arXiv:2202.08850 [gr-qc] .
- [20] V. Bozza, *Phys. Rev. D* **66**, 103001 (2002), arXiv:gr-qc/0208075 .
- [21] V. Cardoso, A. S. Miranda, E. Berti, H. Witek, and V. T. Zanchin, *Phys. Rev. D* **79**, 064016 (2009), arXiv:0812.1806 [hep-th] .
- [22] K. Hioki and K.-i. Maeda, *Phys. Rev. D* **80**, 024042 (2009), arXiv:0904.3575 [astro-ph.HE] .
- [23] L. G. Collodel, B. Kleihaus, and J. Kunz, *Phys. Rev. Lett.* **120**, 201103 (2018), arXiv:1711.05191 [gr-qc] .
- [24] X. Ye and S.-W. Wei, *JCAP* **07**, 049 (2023), arXiv:2301.04786 [gr-qc] .
- [25] P. V. P. Cunha and C. A. R. Herdeiro, *Phys. Rev. Lett.* **124**, 181101 (2020), arXiv:2003.06445 [gr-qc] .
- [26] P. V. P. Cunha, C. Herdeiro, E. Radu, and N. Sanchis-Gual, *Phys. Rev. Lett.* **130**, 061401 (2023), arXiv:2207.13713 [gr-qc] .
- [27] S.-W. Wei and Y.-X. Liu, *Phys. Rev. D* **107**, 064006 (2023), arXiv:2207.08397 [gr-qc] .
- [28] H.-S. Liu, Z.-F. Mai, Y.-Z. Li, and H. Lü, *Sci. China Phys. Mech. Astron.* **63**, 240411 (2020), arXiv:1907.10876 [hep-th] .
- [29] S.-W. Wei, Y.-P. Zhang, Y.-X. Liu, and R. B. Mann, *Phys. Rev. Res.* **5**, 043050 (2023), arXiv:2303.06814 [gr-qc] .
- [30] F. J. Dyson, *Science* **131**, 1667 (1960).
- [31] M. D. Papagiannis, *IAU Symp.* **112**, 543 (1985).
- [32] J. Wright, *Serb.Astron.J.* **200**, 1 (2020).
- [33] B. Aschenbach, *Astron. Astrophys.* **425**, 1075 (2004), arXiv:astro-ph/0406545 .

- [34] K. S. Thorne, *Astrophys. J.* **191**, 507 (1974).
- [35] Z. Stuchlik, P. Slany, G. Torok, and M. A. Abramowicz, *Phys. Rev. D* **71**, 024037 (2005), arXiv:gr-qc/0411091 .
- [36] A. Mueller and B. Aschenbach, *Class. Quant. Grav.* **24**, 2637 (2007), arXiv:0704.3963 [gr-qc] .
- [37] Z. Stuchlik, M. Blaschke, and P. Slany, *Class. Quant. Grav.* **28**, 175002 (2011), arXiv:1108.0191 [gr-qc] .
- [38] A. Tursunov, Z. Stuchlík, and M. Kološ, *Phys. Rev. D* **93**, 084012 (2016), arXiv:1603.07264 [gr-qc] .
- [39] J. Khodagholizadeh, V. Perlick, and A. Vahedi, *Phys. Rev. D* **102**, 024021 (2020), arXiv:2002.04701 [gr-qc] .
- [40] A. Vahedi, J. Khodagholizadeh, and A. Tursunov, *Eur. Phys. J. C* **81**, 280 (2021), arXiv:2103.14912 [gr-qc] .
- [41] S. Hod, *Eur. Phys. J. C* **78**, 417 (2018), arXiv:1811.04948 [gr-qc] .
- [42] B. P. Abbott and et. al. (LIGO Scientific and Virgo Collaboration), *Phys. Rev. Lett.* **118**, 221101 (2017).
- [43] C. de Rham, *Living Rev. Rel.* **17**, 7 (2014), arXiv:1401.4173 [hep-th] .
- [44] G. Dvali, G. Gabadadze, and M. Porrati, *Physics Letters B* **484**, 112 (2000).
- [45] G. Dvali, G. Gabadadze, and M. Porrati, *Physics Letters B* **485**, 208 (2000).
- [46] B. P. Abbott and et. al. (LIGO Scientific Collaboration and Virgo Collaboration), *Phys. Rev. Lett.* **116**, 061102 (2016).
- [47] M. Fierz and W. E. Pauli, *Proceedings of the Royal Society of London. Series A. Mathematical and Physical Sciences* **173**, 211 (1939).
- [48] D. G. Boulware and S. Deser, *Phys. Rev. D* **6**, 3368 (1972).
- [49] E. A. Bergshoeff, O. Hohm, and P. K. Townsend, *Physical Review Letters* **102**, 201301 (2009).
- [50] C. de Rham, G. Gabadadze, and A. J. Tolley, *Phys. Rev. Lett.* **106**, 231101 (2011).
- [51] C. de Rham, G. Gabadadze, and A. J. Tolley, *Physics Letters B* **711**, 190 (2012).
- [52] Y. S. Myung, Y.-W. Kim, T. Moon, and Y.-J. Park, *Phys. Rev. D* **84**, 024044 (2011).
- [53] E. A. Bergshoeff, O. Hohm, J. Rosseel, and P. K. Townsend, *Phys. Rev. D* **83**, 104038 (2011).
- [54] W. Kim, S. Kulkarni, and S.-H. Yi, *Journal of High Energy Physics* **2013**, 41 (2013).
- [55] E. Ayón-Beato, M. Hassaine, and M. M. Juárez-Aubry, *Phys. Rev. D* **90**, 044026 (2014).

- [56] Y. S. Myung, *Advances in High Energy Physics* **2015** (2015).
- [57] S. F. Hassan and R. A. Rosen, *Phys. Rev. Lett.* **108**, 041101 (2012).
- [58] S. F. Hassan, R. A. Rosen, and A. Schmidt-May, *Journal of High Energy Physics* **2012**, 26 (2012).
- [59] Y.-F. Cai, D. A. Easson, C. Gao, and E. N. Saridakis, *Phys. Rev. D* **87**, 064001 (2013).
- [60] H. Kodama and I. Arraut, *Progress of Theoretical and Experimental Physics* **2014** (2014).
- [61] D.-C. Zou, R. Yue, and M. Zhang, *The European Physical Journal C* **77**, 256 (2017).
- [62] L. Tannukij, P. Wongjun, and S. G. Ghosh, *Eur. Phys. J. C* **77**, 846 (2017), arXiv:1701.05332 [gr-qc] .
- [63] T. Katsuragawa, S. Nojiri, S. D. Odintsov, and M. Yamazaki, *Phys. Rev. D* **93**, 124013 (2016).
- [64] E. N. Saridakis, *Classical and Quantum Gravity* **30**, 075003 (2013).
- [65] Y.-F. Cai, C. Gao, and E. N. Saridakis, *JCAP* **10**, 048 (2012), arXiv:1207.3786 [astro-ph.CO] .
- [66] G. Leon, J. Saavedra, and E. N. Saridakis, *Classical and Quantum Gravity* **30**, 135001 (2013).
- [67] K. Hinterbichler, J. Stokes, and M. Trodden, *Physics Letters B* **725**, 1 (2013).
- [68] M. Fasiello and A. J. Tolley, *Journal of Cosmology and Astroparticle Physics* **2013**, 002 (2013).
- [69] K. Bamba, M. W. Hossain, R. Myrzakulov, S. Nojiri, and M. Sami, *Phys. Rev. D* **89**, 083518 (2014).
- [70] D. Vegh, (2013), arXiv:1301.0537 [hep-th] .
- [71] H. Zhang and X.-Z. Li, *Phys. Rev. D* **93**, 124039 (2016).
- [72] J. Xu, L.-M. Cao, and Y.-P. Hu, *Phys. Rev. D* **91**, 124033 (2015).
- [73] S. H. Hendi, B. E. Panah, and S. Panahiyan, *Journal of High Energy Physics* **2015**, 157 (2015).
- [74] S. Hendi, B. E. Panah, and S. Panahiyan, *Classical and Quantum Gravity* **33**, 235007 (2016).
- [75] S. H. Hendi, R. B. Mann, S. Panahiyan, and B. Eslam Panah, *Phys. Rev. D* **95**, 021501 (2017).
- [76] S. Hendi, B. E. Panah, and S. Panahiyan, *Physics Letters B* **769**, 191 (2017).
- [77] A. E. Gümrükçüoğlu, C. Lin, and S. Mukohyama, *Journal of Cosmology and Astroparticle Physics* **2011**, 030 (2011).

- [78] P. Gratia, W. Hu, and M. Wyman, *Phys. Rev. D* **86**, 061504 (2012).
- [79] T. Kobayashi, M. Siino, M. Yamaguchi, and D. Yoshida, *Phys. Rev. D* **86**, 061505 (2012).
- [80] C. Deffayet, *Phys. Lett. B* **502**, 199 (2001), arXiv:hep-th/0010186 .
- [81] C. Deffayet, G. Dvali, and G. Gabadadze, *Phys. Rev. D* **65**, 044023 (2002).
- [82] G. Dvali, G. Gabadadze, and M. Shifman, *Phys. Rev. D* **67**, 044020 (2003).
- [83] G. Dvali, S. Hofmann, and J. Khoury, *Phys. Rev. D* **76**, 084006 (2007).
- [84] C. M. Will, *Living reviews in relativity* **17**, 4 (2014).
- [85] M. Mohseni, *Phys. Rev. D* **84**, 064026 (2011).
- [86] A. Gumrukcuoglu, S. Kuroyanagi, C. Lin, S. Mukohyama, and N. Tanahashi, *Class. Quant. Grav.* **29**, 235026 (2012), arXiv:1208.5975 [hep-th] .
- [87] S. Hendi, G. Bordbar, B. Eslam Panah, and S. Panahiyan, *JCAP* **07**, 004 (2017), arXiv:1701.01039 [gr-qc] .
- [88] C. E. Rhoades and R. Ruffini, *Phys. Rev. Lett.* **32**, 324 (1974).
- [89] B. Eslam Panah and H. L. Liu, *Phys. Rev. D* **99**, 104074 (2019), arXiv:1805.10650 [gr-qc] .
- [90] E. Babichev, L. Marzola, M. Raidal, A. Schmidt-May, F. Urban, H. Veermäe, and M. von Strauss, *JCAP* **09**, 016 (2016), arXiv:1607.03497 [hep-th] .
- [91] Y. Akrami, T. S. Koivisto, and M. Sandstad, *Journal of High Energy Physics* **2013**, 99 (2013).
- [92] Y. Akrami, S. F. Hassan, F. Könnig, A. Schmidt-May, and A. R. Solomon, *Physics Letters B* **748**, 37 (2015).
- [93] C. Bachas and I. Lavdas, *Journal of High Energy Physics* **2018**, 3 (2018).
- [94] M. B. Ahmed, W. Cong, D. Kubizňák, R. B. Mann, and M. R. Visser, *Phys. Rev. Lett.* **130**, 181401 (2023), arXiv:2302.08163 [hep-th] .
- [95] R.-G. Cai, Y.-P. Hu, Q.-Y. Pan, and Y.-L. Zhang, *Phys. Rev. D* **91**, 024032 (2015).
- [96] L. Alberte and A. Khmelnitsky, *Phys. Rev. D* **91**, 046006 (2015).
- [97] Z. Zhou, J.-P. Wu, and Y. Ling, *Journal of High Energy Physics* **2015**, 67 (2015).
- [98] A. Dehyadegari, M. Kord Zangeneh, and A. Sheykhi, *Phys. Lett. B* **773**, 344 (2017), arXiv:1703.00975 [hep-th] .
- [99] S. Hendi, B. Eslam Panah, S. Panahiyan, and M. Momennia, *Phys. Lett. B* **775**, 251 (2017), arXiv:1704.00996 [gr-qc] .

- [100] A. Dehghani and S. H. Hendi, *Class. Quant. Grav.* **37**, 024001 (2020), arXiv:1909.00956 [hep-th] .
- [101] S. H. Hendi, S. Panahiyan, B. Eslam Panah, and M. Momennia, *Annalen Phys.* **528**, 819 (2016), arXiv:1506.07262 [hep-th] .
- [102] A. R. Akbarieh, S. Kazempour, and L. Shao, *Phys. Rev. D* **103**, 123518 (2021), arXiv:2105.03744 [gr-qc] .
- [103] P. K. Yerra and C. Bhamidipati, *Phys. Lett. B* **819**, 136450 (2021), arXiv:2007.11515 [hep-th] .
- [104] P. K. Yerra and C. Bhamidipati, *Int. J. Mod. Phys. A* **35**, 2050120 (2020), arXiv:2006.07775 [hep-th] .
- [105] P. K. Yerra and C. Bhamidipati, *Phys. Rev. D* **104**, 104049 (2021), arXiv:2107.04504 [gr-qc] .
- [106] M. Högsås and E. Mörtzell, (2021), arXiv:2106.09030 [astro-ph.CO] .
- [107] A. Caravano, M. Lüben, and J. Weller, (2021), arXiv:2101.08791 [gr-qc] .
- [108] M. Chabab, H. El Moumni, S. Iraoui, and K. Masmar, *Eur. Phys. J. C* **79**, 342 (2019), arXiv:1904.03532 [hep-th] .
- [109] B. Wu, C. Wang, Z.-M. Xu, and W.-L. Yang, (2020), arXiv:2006.09021 [gr-qc] .
- [110] C. de Rham, G. Gabadadze, and A. J. Tolley, *Phys. Rev. Lett.* **106**, 231101 (2011), arXiv:1011.1232 [hep-th] .
- [111] S. G. Ghosh, L. Tannukij, and P. Wongjun, *Eur. Phys. J. C* **76**, 119 (2016), arXiv:1506.07119 [gr-qc] .
- [112] S. H. Hendi, K. Jafarzade, and B. Eslam Panah, *JCAP* **02**, 022 (2023), arXiv:2206.05132 [gr-qc] .
- [113] S.-W. Wei and Y.-X. Liu, *Phys. Dark Univ.* **43**, 101409 (2024), arXiv:2308.11883 [gr-qc] .
- [114] S. Panpanich, S. Ponglertsakul, and L. Tannukij, *Phys. Rev. D* **100**, 044031 (2019), arXiv:1904.02915 [gr-qc] .
- [115] M. Riojas and H.-Y. Sun, (2023), arXiv:2307.06415 [hep-th] .
- [116] D. Berenstein, Z. Li, and J. Simon, *Class. Quant. Grav.* **38**, 045009 (2021), arXiv:2009.04500 [hep-th] .